

Synthesis of new (Bi, La)₃MSb₂O₁₁ phases (M = Cr, Mn, Fe) with KSbO₃-type structure and their magnetic and photocatalytic properties

K RAMESHA*, A S PRAKASH, M SATHIYA, GIRIDHAR MADRAS[†] and A K SHUKLA[†]

CSIR Central Electrochemical Research Institute-Madras Unit, CSIR-Madras Complex, Taramani, Chennai 600 113, India

[†]Solid State and Structural Chemistry Unit, Indian Institute of Science, Bangalore 560 012, India

MS received 26 October 2010; revised 14 December 2010

Abstract. Synthesis and structure of new (Bi, La)₃MSb₂O₁₁ phases (M = Cr, Mn, Fe) are reported in conjunction with their magnetic and photocatalytic properties. XRD refinements reflect that Bi₃CrSb₂O₁₁, Bi₂LaCrSb₂O₁₁, Bi₂LaMnSb₂O₁₁ and Bi₂LaFeSb₂O₁₁ adopt KSbO₃-type structure (space group, $Pn\bar{3}$). The structure can be described through three interpenetrating networks where the first is the (M/Sb)O₆ octahedral network and other two are the identical networks having Bi₆O₄ composition. The magnetic measurements on Bi₂LaCrSb₂O₁₁ and Bi₂LaMnSb₂O₁₁ show paramagnetic behaviour with magnetic moments close to the expected spin only magnetic moments of Cr⁺³ and Mn⁺³. The UV-Visible diffuse reflectance spectra are broad and indicate that these materials possess a bandgap of ~ 2 eV. The photocatalytic activity of these materials has been investigated by degrading Malachite Green (MG) under exposure to UV light.

Keywords. A₃B₃O₁₁; KSbO₃; magnetism; synthesis; crystal structure; photocatalysis.

1. Introduction

A₃B₃O₁₁ compounds crystallizing in KSbO₃-type structure exhibit interesting properties such as ionic conductivity and electrocatalysis (Gokagac and Kennedy 1993; He *et al* 1997). Both perovskite and KSbO₃ structures have the same chemical formula, ABO₃. But, unlike the perovskite structure, the KSbO₃ structure has characteristic tunnel arrangement, which has been ascribed to large covalent character of B–O bonds that restrict the formation of ~ 180° B–O–B angles (Goodenough and Kafalas 1973; Hong *et al* 1974). A₃B₃O₁₁ is a subset / compositional variant of KSbO₃-family that also has the tunnel motif. A₃B₃O₁₁ is made up of three interpenetrating lattices (Sleight and Bouchard 1973). However, only a few members of this family are known and their physical properties have not been well studied. Sleight and Bouchard (1973) were the first to report new compounds such as Bi₃GaSb₂O₁₁ of A₃B₃O₁₁ family and observed large thermal factor for Bi. Variable temperature neutron diffraction studies showed that positional site disorder and open geometry are responsible for the observed large thermal parameters of Bi (Ismunandar *et al* 1998). Bi₃Ru₃O₁₁ is another important member of the family which shows Ru–Ru bonding (Abraham and Thomas 1975), while La₃Ru₃O₁₁ does not have direct bonding between Ru–Ru (Cotton and Rice 1978; Khalifah and Cava 2001). Recently, synthesis of a new member of this family, viz. Bi₃Mn₃O₁₁, is reported (Belik and Muromachi 2009). Interestingly, Bi₃Mn₃O₁₁ with ran-

domly distributed Mn⁺³ and Mn⁺⁵ ions exhibits high ferri-magnetism with T_c at ~ 150 K. Accordingly, A₃B₃O₁₁ family of oxides crystallizing in KSbO₃-type structure displays interesting and diverse properties owing to their remarkable structure and bonding.

Many of Sb⁺⁵ containing oxides such as Ca₂Sb₂O₇, CaSb₂O₆, NaSbO₃ (Abraham *et al* 1974) and AgSbO₃ (Singh and Uma 2009) have been investigated for their photocatalytic properties owing to their wide delocalized conduction band. Further, Bi⁺³ containing oxides Bi₂WO₆ (Sato *et al* 2002), BiVO₄ (Zhang and Zhu 2005), Bi₂Ti₂O₇ (Li *et al* 2008) exhibit photocatalytic activity on exposure to visible light. This suggests that Sb⁺⁵ and Bi⁺³ have the ability to induce photocatalysis in oxides. Indeed, BiSbO₄ (Lin *et al* 2006) shows good photocatalytic activity towards the degradation of methylene blue (MB) on exposure to both UV and visible light. Photocatalysis is a viable environmentally benign process that can be used for destruction of organic matter in effluents (Frank and Bard 1977). Malachite green (MG), a triarylmethane dye, is widely used as a biocide in the aquaculture industry as well as a dye in the silk, wool, cotton, leather, paper and acrylic industries. It is also employed as a food additive and a medical disinfectant. Despite its extensive use, MG is highly undesirable due to its toxic properties which are known to cause carcinogenesis, mutagenesis, teratogenicity and respiratory toxicity (Srivastava *et al* 2004). Recent studies have dealt with the light-induced degradation of MG by means of UV-A irradiation in TiO₂ aqueous suspensions (Kominami *et al* 2003), and UV-C irradiation in presence of hydrogen peroxide (Modirshahla and Behnajady 2006).

* Author for correspondence (ramesha.cecri@gmail.com)

In this study, synthesis, structure and magnetic properties of four new members of $A_3B_3O_{11}$ family adopting $KSbO_3$ -type structure, viz. $Bi_3CrSb_2O_{11}$, $Bi_2LaCrSb_2O_{11}$, $Bi_2LaMnSb_2O_{11}$, and $Bi_2LaFeSb_2O_{11}$ are reported. For the purpose of comparison, we have also prepared $Bi_3FeSb_2O_{11}$ reported elsewhere (Sleight and Bouchard 1973). The study also reports the photocatalytic activity of $(Bi, La)_3MSb_2O_{11}$ oxides.

2. Experimental

2.1 Synthesis

Polycrystalline samples with composition $(Bi, La)_3MSb_2O_{11}$ where $M = Cr, Mn, Fe$ were synthesized by the solid state synthesis method. Stoichiometric quantities of Bi_2O_3 , La_2O_3 , M_2O_3 ($M = Cr, Mn$ or Fe) and Sb_2O_3 were mixed thoroughly and heated in air at $1000^\circ C$ for 24 h followed by heating at $1100^\circ C$ for 24 h with one intermediate grinding and pelletizing.

2.2 Characterization

X-ray powder diffraction (XRD) patterns for the oxide samples were recorded using Philips (Xpert PRO) diffractometer using CuK_α radiation. Rietveld quality data were collected with a step size of 0.02° over 12 h and refinements were carried out using General Structure Analysis System (GSAS) code (Larson and Von Dreele 2000) and EXPGUI (Toby 2001) interface. A Pseudo-Voigt function was used to model peak profile and background was fitted with Chebyshev function.

For selected samples, magnetization measurements were carried out using PPMS (Quantum Design) magnetometer in the temperature range 5–300 K at $H = 1000$ Oe magnetic field. Both zero field cooled (ZFC) and field cooled (FC) data were collected. ZFC magnetic data were recorded in a field of 1000 Oe upon warming from 5K after cooling from room temperature under zero fields. FC magnetic data were also collected upon warming from 5K, but subsequently the samples were cooled under a 1000 Oe field. Magnetization versus field (M vs H) measurements were carried out at 5 K up to a maximum field of 5 Tesla.

The morphology and particle size were analysed using scanning electron microscope (JEOL-JSM-5600LV, 20 kV) attached with EDAX facility for elemental analysis. The UV-Visible diffuse reflectance spectra (DRS) for the powder sample were recorded using UV-Visible spectrometer (Lambda 32 Perkin Elmer).

2.3 Dye materials for photodegradation studies

Malachite green (MG) was procured from S.D. Fine Chemicals, India with more than 99% purity and was used without

further purification. Water was double distilled and filtered through Millipore membrane filter prior to use.

2.4 Photodegradation experiments

The photocatalytic activity of compounds was studied under UV radiation. A high-pressure mercury vapour lamp (HPML) of 125 W (Philips, India) was used as UV source. The lamp radiated predominantly at 365 nm with an incident intensity of 10^{-6} Einstein $L^{-1} s^{-1}$ and a photon flux of $25 W m^{-2}$, which was measured by *o*-nitrobenzaldehyde actinometry. The design and operation of the photochemical reactor used in the study are discussed elsewhere (Aarthi and Madras 2007).

In a typical experiment, aqueous solution containing known concentration of dye (50 ppm) and catalyst (loading of 1 g/L) were taken in the photoreactor. The suspended catalyst and dye solutions were continuously stirred with a magnetic stirrer. The pH of the solution was not adjusted during the experiment and the experiments were conducted at the natural pH. The degradation under UV light in presence of the catalyst was carried out for 1 h during which samples were collected at regular intervals of time.

The collected samples were then filtered and centrifuged to remove any catalyst particles before the UV-Visible analysis. All dyes were analysed with a UV-Visible spectrometer (Lambda 32 Perkin-Elmer) between 200 and 800 nm. The calibration was based on the Beer-Lambert law at their maximum absorption wavelength, λ_{max} .

Experiments were initially conducted only with UV without any catalyst (photolysis) and with catalyst without any UV exposure (dark), and no degradation was observed in these cases. All experiments were conducted thrice and the average difference in concentration was less than ± 2 ppm.

3. Results and discussion

3.1 Phase identification and XRD Rietveld refinements

Figure 1 shows the XRD patterns for $(Bi, La)_3MSb_2O_{11}$ phases where $M = Cr, Mn, Fe$. Preliminary indexing and phase identification reveal the formation of single phases with $KSbO_3$ type structure. Further, Rietveld refinements were carried out using $Bi_3GaSb_2O_{11}$ as model structure (Sleight and Bouchard 1973; Ismunandar *et al* 1996) with space group $Pn\bar{3}$. In $Bi_3GaSb_2O_{11}$, the six atoms have the following positions: Bi(1) at $8e(x, x, x)$, Bi(2) at $4b(0, 0, 0)$, Ga/Sb at $12g(x, \frac{3}{4}, \frac{1}{4})$, O(1) at $8e(x, x, x)$, O(2) at $12f(x, \frac{1}{4}, \frac{1}{4})$ and O(3) at $24h(x, y, z)$. For La containing compositions, best Rietveld fit were obtained when La was disordered at both Bi(1) and Bi(2) positions with equal site occupancy. Distributing all La at $4b$ position resulted in higher agreement factors. So Bi atoms occupying both $8e$ and $4b$ positions is crucial for stabilizing the structure. This was further confirmed by our attempts to prepare $BiLa_2MSb_2O_{11}$

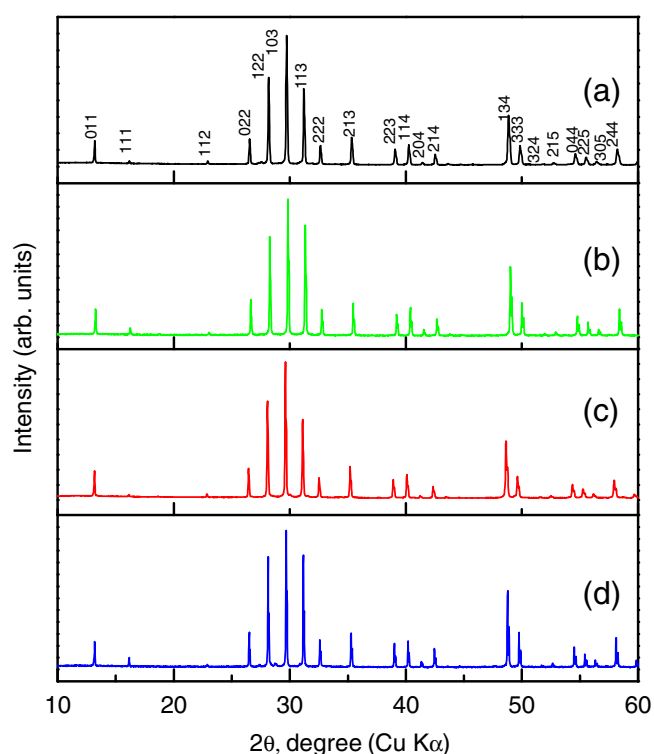


Figure 1. Powder X-ray diffraction patterns for compounds crystallizing in K SbO₃-type structure: (a) Bi₂LaCrSb₂O₁₁, (b) Bi₃CrSb₂O₁₁, (c) Bi₂LaMnSb₂O₁₁ and (d) Bi₂LaFeSb₂O₁₁. (*hkl*) indexing of peaks is shown in the top panel.

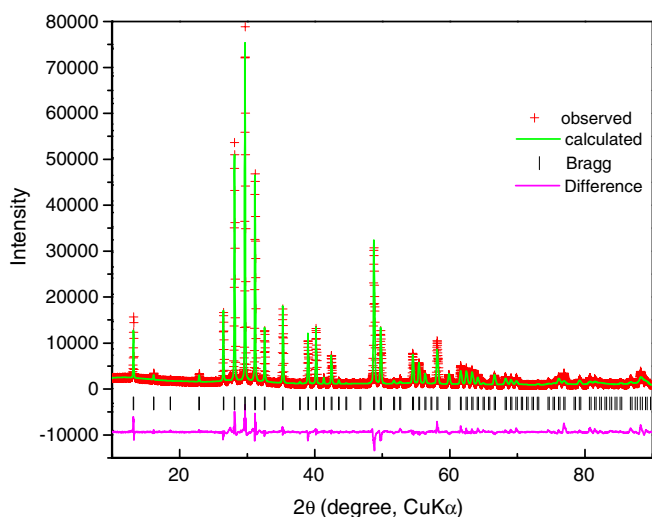


Figure 2. Powder XRD Rietveld fit for Bi₂LaCrSb₂O₁₁.

compounds by increasing La content in lieu of Bi, which resulted in additional impurity phases. The Rietveld fit for Bi₂LaCrSb₂O₁₁ is shown in figure 2 as a representative example. The crystallographic data and bond lengths are given in tables 1 and 2. The lattice parameters of all the compositions obtained from XRD Rietveld refinements are listed in table 3.

Table 1. Crystallographic data for Bi₂LaCrSb₂O₁₁.

Atom	Position	<i>x</i>	<i>y</i>	<i>z</i>	<i>B</i> (Å) ²
Bi(1)	8e	0.3821	0.3821	0.3821	1.22(3)
Bi(2)	4b	0	0	0	0.94(2)
Cr, Sb	12g	0.5949	0.75	0.25	0.63(2)
O1	8e	0.1367	0.1367	0.1367	0.84(3)
O2	12g	0.6023	0.25	0.25	0.78(3)
O3	24h	0.5937	0.5314	0.2471	0.67(1)

Cubic, space group $Pn\bar{3}$, $a = 9.506(3)$ Å, $R_{wp} = 8.81$, $\chi^2 = 3.44$.

Table 2. Interatomic distances (Å) for Bi₂LaCrSb₂O₁₁.

Bi1–O1 (×3)	2.346(1)	Cr/Sb–O2 (×2)	2.036(1)
Bi1–O2 (×3)	2.745(1)	Cr/Sb–O3 (×2)	2.070(1)
Bi1–O3 (×3)	2.776(1)	Cr/Sb–O3 (×2)	1.910(1)
Bi2–O1 (×2)	2.251(1)		
Bi2–O3 (×6)	2.529(2)		

Table 3. Lattice parameters for (Bi, La)₃MSb₂O₁₁ compounds.

Compound	Lattice parameter, <i>a</i> (Å)
Bi ₂ LaCrSb ₂ O ₁₁	9.506(3)
Bi ₃ CrSb ₂ O ₁₁	9.478(2)
Bi ₂ LaMnSb ₂ O ₁₁	9.546(2)
Bi ₂ LaFeSb ₂ O ₁₁	9.523(3)
Bi ₃ FeSb ₂ O ₁₁	9.516(3)

Our efforts to synthesize Bi₃MnSb₂O₁₁ and Bi₃NiSb₂O₁₁ in K SbO₃ type structure were unsuccessful. Instead, pyrochlore phases (Ramesha *et al* 2003a, b) were obtained as revealed from their powder XRD patterns. The formation of pyrochlore phase implies that Mn is in +2 oxidation state (instead of +3) corresponding to the chemical formula, Bi₂Mn_{0.67}Sb_{1.33}O₇.

3.2 Crystal structure

The structure essentially can be viewed as three interpenetrating networks (figure 3). The M and Sb form octahedral network with oxygen similar to that found in K SbO₃. The MSb₂O₉ array consists of pair of edge sharing octahedra and every such unit is further connected through vertices to form 3-dimensional network (figure 3a). The other two identical networks (figure 3b) contain only Bi and O1 atoms. Four Bi(2) atoms form a tetrahedron that contain O(1) on every face. The Bi(1) atom is connected to two such tetrahedron through O(1). Two such networks with a formula, Bi(2)₄O(1)₄Bi(1)₂, interpenetrate the MSb₂O₉ octahedral network. The entire Bi-oxygen network can also be described as corner sharing Bi₈O₄ stellate quadrangulae formed by four Bi(1)₃Bi(2) tetrahedra each containing O1, in

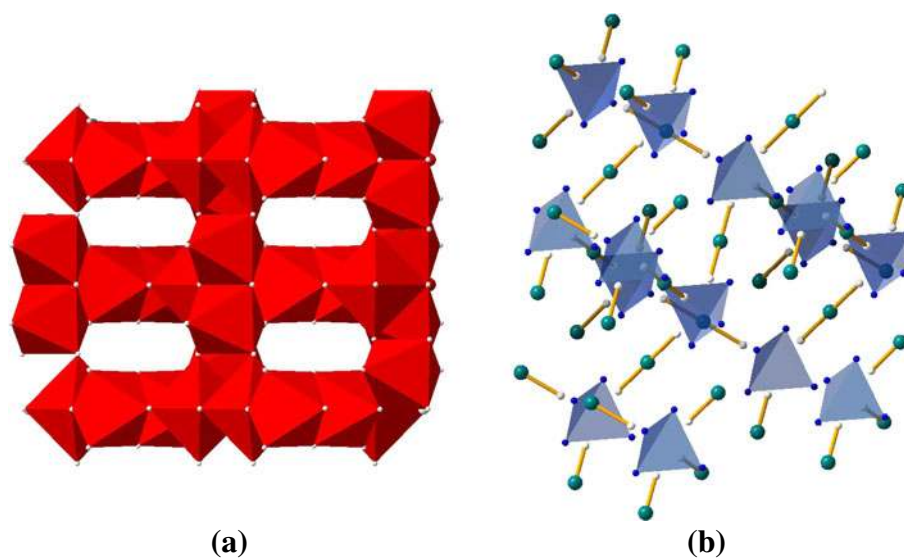


Figure 3. Crystal structure of $(\text{Bi, La})_3\text{MSb}_2\text{O}_{11}$ showing interpenetrating networks. (a) $\text{MSb}_2\text{O}_{11}$ octahedral network with M–Sb atoms at the centre and oxygen atoms at corners of octahedra, (b) two identical Bi_6O_4 networks where Bi(2) atoms (blue) form tetrahedron that contain O(1) atom (white) on every face. The Bi(1) atoms (green) are connected to two such tetrahedron through O(1).

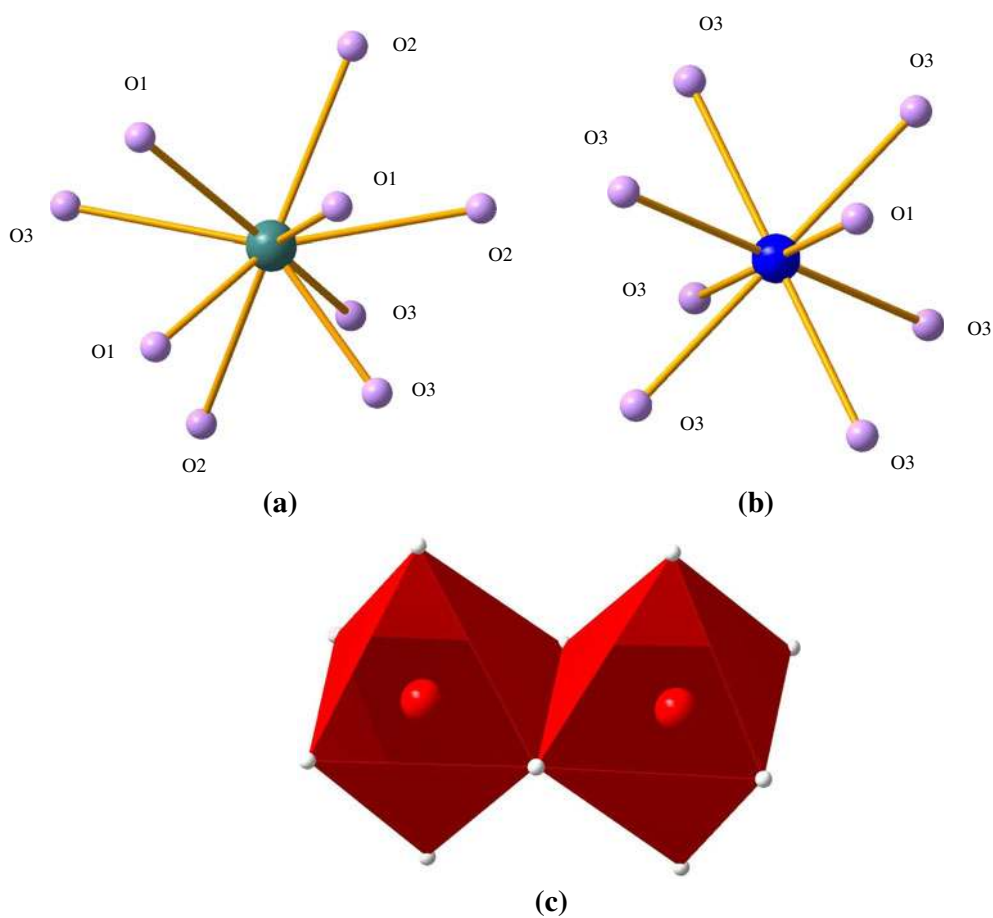


Figure 4. Ball-and-stick drawing for (a) the coordination of Bi(1)O₉ polyhedron, (b) Bi(2)O₈ coordination and (c) edge shared $(\text{MSb}_2)\text{O}_9$ octahedra.

turn sharing Bi(1)₃ face with fifth empty Bi(1)₄ tetrahedron (Ismunandar *et al* 1996).

Figure 4 shows the ball-and-stick drawing of the oxygen coordination sphere around Bi(1), Bi(2) and (M/Sb₂). Bi(1) atoms connected to 9 oxygen atoms form a tricapped trigonal prism while Bi(2) has 8-fold coordination similar to that found in pyrochlores. The structure of Bi₃GaSb₂O₁₁ has been discussed in detail elsewhere (Sleight and Bouchard 1973; Ismunandar *et al* 1996). In contrast to the Bi₃GaSb₂O₁₁ structure, the O1 atoms are absent in KSbO₃ and K atoms lie in the cavity formed by SbO₃ framework.

3.3 Magnetic properties

In (Bi, La)₃MSb₂O₁₁ (M = Cr, Mn, Fe) compositions, only M atoms are the magnetic species, which are statically distributed in the MSb₂O₉ network. Accordingly, only para-

magnetic behaviour can be expected. The χ_M^{-1} vs T plots for Bi₂LaCrSb₂O₁₁ and Bi₂LaMnSb₂O₁₁ are shown in figure 5 with M vs H behaviour at 5 K in the inset. As expected, the χ_M^{-1} vs T behaviour is linear for both the compounds, confirming paramagnetic interaction. The ZFC and FC data converge, and there is no separation between FC and ZFC curves down to 5K. For Cr composition, the plot is linear (figure 5a) and fits well to Curie behaviour ($\theta = 0$) in the temperature range 5–280K. The spin-only magnetic moment obtained is 3.65 μ_B which is slightly smaller than calculated spin-only moment for 3 unpaired spins; expected μ_{eff} for Cr³⁺ being 3.9 μ_B . The χ_M^{-1} vs T plot for Mn composition (figure 5b) follows Curie–Weiss law. A linear fit between 50 K and 300 K yields $\theta = -7.4$ K, and $\mu_{\text{eff}} = 4.7 \mu_B$; the calculated μ_{eff} value for spin-only Mn³⁺ (d^4) being 4.9 μ_B . There is a small deviation of slope below 10 K with θ becoming zero. The M vs H plots at 5 K (insets to figures 5a–b) are typical Brillouin functions for the magnetization of paramagnets.

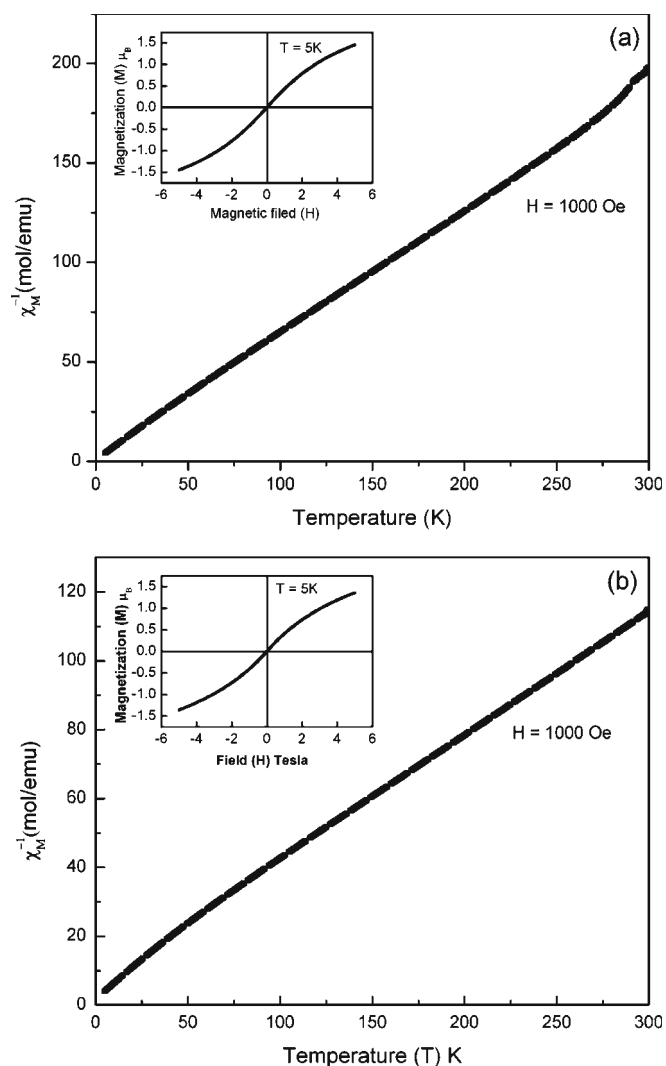


Figure 5. χ_M^{-1} vs T plots for (a) Bi₂LaCrSb₂O₁₁ and (b) Bi₂LaMnSb₂O₁₁. The M vs H data at 5K are shown as inset.

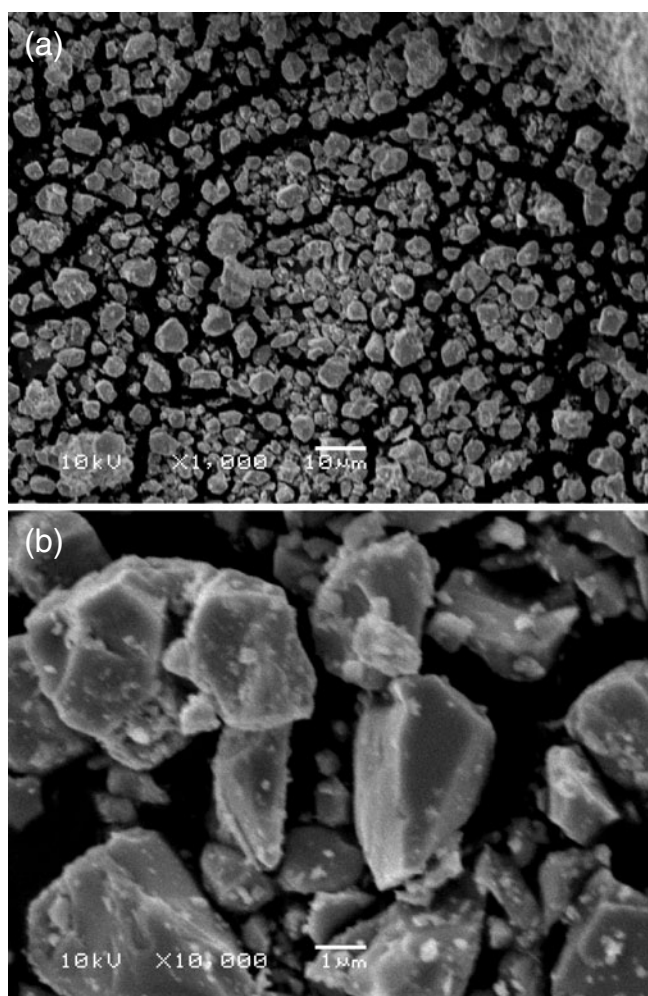


Figure 6. SEM micrographs for Bi₂LaMnSb₂O₁₁ at two different magnifications.

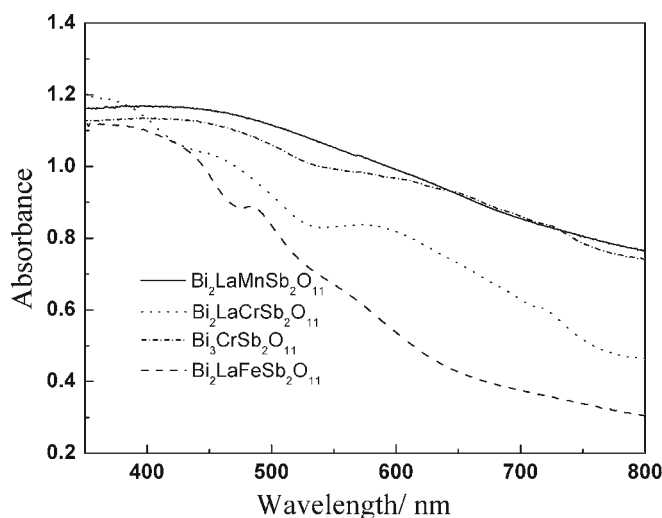


Figure 7. UV-Vis diffuse-reflectance spectra for $(\text{Bi, La})_3\text{MSb}_2\text{O}_{11}$ ($\text{M} = \text{Cr, Mn, Fe}$) compounds.

3.4 SEM and DRS

The scanning electron micrographs for $\text{Bi}_2\text{LaMnSb}_2\text{O}_{11}$ phase are shown in figures 6(a) and (b). The micron-sized particles are depicted in the micrographs. The EDAX spectrum recorded on various crystallites confirms the cation stoichiometry. Figure 7 shows the diffuse-reflectance spectra (DRS) of the members. DRS reveals that $(\text{Bi, La})_3\text{MSb}_2\text{O}_{11}$ compounds show broad absorption in the UV-Visible range similar to that found for BiVO_4 (Kudo *et al* 1999), BiCu_2VO_6 (Liu *et al* 2005), Ag_2CrO_4 (Ouyang *et al* 2008), $\text{CsLaSrNb}_2\text{NiO}_9$ (Yao and Ye 2006) oxides, which are excellent photocatalysts. It is noteworthy that the onset of absorption edges (figure 7) is unclear because of several absorption overlaps in the visible range. For instance, the spectra for $\text{Bi}_2\text{LaFeSb}_2\text{O}_{11}$ indicate that there would be more than two absorption edges with main absorption edge at around 600 nm ($E_g = 2.07$ eV). In addition, there are two more absorption edges around 630 nm ($E_g = 1.97$ eV) and 700 nm ($E_g = 1.77$ eV). Similarly two absorption edges could be identified for $\text{Bi}_2\text{LaCrSb}_2\text{O}_{11}$ at 670 nm (1.85 eV) and 710 nm (1.75 eV).

The band structure of oxides is generally defined by metal d -level and O $2p$ level, the valence band is assumed to be O $2p$ level and the metal d -levels constitute the conduction band (Scaife 1980). Absorption of photons with an energy equal to or greater than bandgap generates electron-hole pairs. When oxides contain transition metals with partially filled d -orbitals, the electronic structure is strongly influenced by the transition metals (Wang *et al* 2003; Yao and Ye 2006). The visible light response of such compounds is attributed to the splitting of d -orbitals in octahedral field that creates new band levels in the bandgap (Wang *et al* 2003; Yin *et al* 2003). The two or more absorption edges observed in the DRS spectra of $\text{Bi}_2\text{LaFeSb}_2\text{O}_{11}$ or

$\text{Bi}_2\text{LaCrSb}_2\text{O}_{11}$ indicate that additional energy levels have been created due to the partially filled d -orbitals of Fe^{+3} or Cr^{+3} . From the band structure of Bi^{+3} and Sb^{+5} containing compounds (Lin *et al* 2006), one can constitute the band structure of $(\text{Bi, La})_3\text{MSb}_2\text{O}_{11}$ compounds as follows: the valence band mainly composed of O $2p$ orbitals hybridized by Bi $6s$ and Sb $4d$ orbitals. The conduction band primarily consists of Sb $5s$ and Bi $6p$ orbitals. The hybrid states in valence band as well as conduction band and their s character imply a high mobility of photogenerated charge carriers favouring photocatalytic property (Kim *et al* 2004; Tang *et al* 2007).

3.5 Photocatalysis

MG is a non-volatile and highly soluble compound and hydroxyl radical mediated reactions are likely to occur primarily in the liquid bulk. Because these reactions occur at relatively low substrate concentrations, they can usually be described by a pseudo-first order kinetic expression:

$$\frac{dC}{dt} = kt.$$

The above relationship can be solved to obtain $C/C_0 = e^{-kt}$ where C is the concentration of the dye, C_0 the initial concentration of the dye, t the time and k the rate constant. The degradation profile for the dye and the degradation rate constant are shown in figure 8. It is clear that the dye is degraded in presence of the catalyst. It is also clear that the degradation in presence of $\text{Bi}_2\text{LaMnSb}_2\text{O}_{11}$ is highest.

The photocatalytic property depends on the crystal structure. Tunnel structures or distorted structures generally

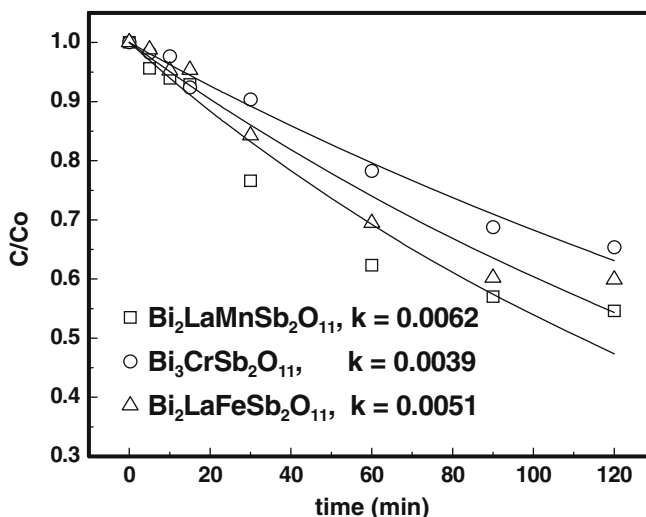


Figure 8. Degradation profile of Malachite green (MG) dye in presence of catalyst material $\text{Bi}_2\text{LaMnSb}_2\text{O}_{11}$, $\text{Bi}_3\text{CrSb}_2\text{O}_{11}$ and $\text{Bi}_2\text{LaFeSb}_2\text{O}_{11}$ under UV light. C_0 is the initial concentration and C the concentration at time, t . The lines fitted by the first order rate and the rate constant (k) are also indicated.

promote catalytic property as for BaTi₄O₉ and A₂Ti₆O₁₃ (A = Na, K) compounds (Templeton and Dauben 1960; Hofmeister *et al* 1984; Kohno *et al* 2000). Such structures possess dipole moment that facilitates photogeneration of carriers, their efficient separation and transport. Accordingly, the photocatalytic property of (Bi, La)₃MSb₃O₁₁ compounds can be related to their tunnel structure that contains highly distorted (M/Sb)O₆, Bi(1)O₉ and Bi(2)O₈ polyhedra. For instance, in Bi₂LaCrSb₂O₁₁ there are three types of Bi(1)–O distances (2.346, 2.745, 2.776 Å) and two types of Bi(2)–O distances (2.251, 2.529 Å). The (Cr/Sb)₂O₉ units that form three-dimensional tunnel structure consists of a pair of edge sharing distorted (Cr/Sb)O₆ octahedra, which exhibit three types of Cr/Sb–O bond distances (2.036, 2.070 and 1.910 Å). The presence of such distorted units induces dipole moment in the structure, which enables formation of photo-generated charge carriers and their effective separation (Sato *et al* 2002; Lin *et al* 2006). In addition, the hybrid nature of valence band and conduction band also favours the high mobility of charge carriers (Tang *et al* 2007).

4. Conclusions

New members of A₃B₃O₁₁ family with composition (Bi, La)₃MSb₂O₁₁ are synthesized and their structure determined by XRD Rietveld refinements. Bi₃CrSb₂O₁₁, Bi₂LaCrSb₂O₁₁, Bi₂LaMnSb₂O₁₁, and Bi₂LaFeSb₂O₁₁ compositions adopt KSbO₃-type structure. The magnetic measurements on Bi₂LaCrSb₂O₁₁ and Bi₂LaMnSb₂O₁₁ samples showed paramagnetic behaviour. The observed μ_{eff} values are 3.65 and 4.7 μ_{B} , respectively which are close to the calculated spin-only moments for Cr⁺³ (*d*³) and Mn⁺³ (*d*⁴) ions. Bi₃MnSb₂O₁₁ and Bi₃NiSb₂O₁₁ do not form KSbO₃-type structure and, instead, adopt pyrochlore phases. The photocatalytic properties of (Bi, La)₃MSb₂O₁₁ compounds are investigated by degrading a dye, Malachite green, under UV light. The study indicates that compounds studied here are photocatalytically active.

References

- Aarthi T and Madras G 2007 *Ind. Eng. Chem. Res.* **46** 7
 Abraham F and Thomas D 1975 *Bull. Soc. Fr. Mineral Crystallogr.* **98** 25
 Abraham F, Nowogrocki G and Thomas D 1974 *C.R. Seances Acad. Sci., Ser. C* **278** 421
 Belik A A and Muromachi E T 2009 *J. Am. Chem. Soc.* **131** 9504
 Cotton F A and Rice C E 1978 *J. Solid State Chem.* **25** 137
 Frank S N and Bard A J 1977 *J. Am. Chem. Soc.* **99** 303
 Gokagac G and Kennedy B J 1993 *Langmuir* **9** 1862
 Goodenough J B and Kafalas J K 1973 *J. Solid State Chem.* **6** 493
 He L, Anderson J, Franzen H F and Johnson D C 1997 *Chem. Mater.* **9** 715
 Hofmeister W, Tillmanns E and Bauer W H 1984 *Acta Crystallogr. C* **40** 1510
 Hong H Y-P, Kafalas J A and Goodenough J B 1974 *J. Solid State Chem.* **9** 345
 Ismunandar, Kennedy B J and Hunter B A 1996 *J. Solid State Chem.* **127** 178
 Ismunandar, Kennedy B J and Hunter B A 1998 *Solid State Commun.* **108** 649
 Khalifah P and Cava R J 2001 *Phys. Rev.* **B64** 085111
 Kim H G, Hwang D W and Lee J S 2004 *J. Am. Chem. Soc.* **126** 8912
 Kohno M, Ogura S, Sato K and Inoue Y 2000 *Chem. Phys. Lett.* **319** 451
 Kominami H, Kumamoto H, Kera Y and Ohtani B 2003 *J. Photochem. Photobiol.* **A160** 99
 Kudo A, Omori K and Kato H 1999 *J. Am. Chem. Soc.* **121** 11459
 Larson A C and Von Dreele R B 2000 Los Alamos National Laboratory Report No. LAUR86-748
 Li G, Zhang D and Yu J C 2008 *Chem. Mater.* **20** 3983
 Lin X P, Huang F U, Wang W D and Zhang K L 2006 *Appl. Catal.* **A307** 257
 Liu H, Nakamura R and Nakato Y 2005 *Chem. Phys. Chem.* **6** 2499
 Modirshahla N and Behnajady M A 2006 *Dyes Pigments* **70** 54
 Ouyang Z, Li Z, Ouyang Z, Yu T, Ye J and Zou Z 2008 *J. Phys. Chem.* **C112** 3134
 Ramesha K, Sebastian L, Eichhorn B and Gopalakrishnan J 2003a *J. Mater. Chem.* **13** 2011
 Ramesha K, Sebastian L, Eichhorn B and Gopalakrishnan J 2003b *Chem. Mater.* **15** 668
 Sato J, Saito N, Nishiyama H and Inoue Y 2002 *J. Photochem. Photobiol.* **A148** 85
 Scaife D E 1980 *Sol. Energy* **25** 41
 Singh J and Uma S 2009 *J. Phys. Chem.* **C 113** 12483
 Sleight A W and Bouchard R 1973 *Inorg. Chem.* **12** 2314
 Srivastava S, Sinha R and Roy D 2004 *Aquat. Toxicol.* **66** 319
 Tang J, Zou Z and Ye J 2007 *J. Phys. Chem.* **C111** 12779
 Templeton D H and Dauben C H 1960 *J. Chem. Phys. Lett.* **32** 1515
 Toby B H 2001 *J. Appl. Crystallogr.* **34** 210
 Wang W, Zou Z and Ye J 2003 *Chem. Phys. Lett.* **373** 191
 Yao W and Ye J 2006 *Catal. Lett.* **110** 139
 Yin J, Zou Z and Ye J 2003 *J. Phys. Chem.* **B107** 4936
 Zhang C and Zhu Y 2005 *Chem. Mater.* **17** 3537